

In Situ Visualization of Interfacial Sodium Transport and Electrochemistry between Few-Layer Phosphorene

Chongyang Zhu, Ruiwen Shao, Shulin Chen, Ran Cai, Yi Wu, Libing Yao, Weiwei Xia, Meng Nie, Litao Sun,* Peng Gao,* Huolin L. Xin, and Feng Xu*

For rechargeable batteries, ionic transport within the electrode materials is a critical process that controls the rate capability and energy efficiency of the battery. Despite substantial studies, the atomistic observation of the interfacial ionic transport and electrochemical reactions occurring between the solid-state electrodes is lacking. Here, in situ transmission electron microscopy (TEM) is used to deliberately design an unusual sample configuration, enabling dynamic observation of the sodium ionic transport within a single-crystal nanostructure and between different few-layer phosphorene nanosheets. An unhindered and reversible ionic shuttling between few-layer phosphorene is directly observed in real time. In addition, it is found that sodium transport kinetics are closely related to the interface orientation and the intimate contact between solid electrodes plays a significant role in inhibiting dendrite growth. Furthermore, by fast TEM imaging with ≈ 40 ms resolution a unique stripe-like sodium transport behavior is observed in phosphorene, and the multiple sodium ionic transport pathways at the interfaces with atomic spatial resolution are revealed. This work may supply enlightening insights into understanding the solid–solid interfacial electrochemistry between electrode materials.

advanced rechargeable batteries have been the focus of this issue.^[7–9] Particularly, the solid–solid interfaces within active electrodes materials are of great significance in controlling ionic transfer kinetics and affecting the battery performance.^[8,10,11]

The solid–solid interfacial ionic transport inside a battery has been studied by both experiments and calculations.^[11–17] It is reported that the lattice mismatch within solid-state electrolyte grain boundaries brings about high “grain-boundary” resistance, leading to low Li^+ transport kinetics in whole batteries.^[12] Besides, a space charge layer formed at the heterointerface also shows large diffusion impedance and is regarded to be rate-determining.^[13–15] In addition, it has demonstrated that the poor compatibility between electrolyte and electrodes gives rise to the large chemical bond change and insufficient contact area with limited ionic transport pathways during cycling, ultimately impeding the ions transport.^[16,17] Despite the extensive


1. Introduction

Surface and interfacial chemistry is of fundamental importance in functional nanomaterials applied in catalysis,^[1] energy storage and conversion,^[2–4] sensors,^[5] and other nanotechnologies.^[6] It has been a perpetual challenge for the scientific community to gain accurate and comprehensive pictures of the structures, dynamics, and interactions at interfaces. In this regard, interfacial ionic transport and reactions in

research and productive progress, few work has been dedicated to the study of the solid–solid interfaces between electrode materials, which are destined to be one of ionic transport pathways due to the intimate contacts. Particularly, it has been recently reported that individual nanocrystals can be precisely achieved by the electrically driven ionic exchange.^[18] Accordingly, mass transfer and electrochemical reactions are expected to occur at these interfaces during charging or discharging of the battery. To this end, real-time and atomic-scale probing

Dr. C. Y. Zhu, Dr. R. Cai, Dr. Y. Wu, Dr. L. B. Yao, Dr. W. W. Xia, Prof. M. Nie, Prof. L. T. Sun, Prof. F. Xu
SEU-FEI Nano-Pico Center
Key Laboratory of MEMS of the Ministry of Education
Southeast University
Nanjing 210096, China
E-mail: slt@seu.edu.cn; fxu@seu.edu.cn

Dr. R. W. Shao
Key Laboratory of Photochemical Conversion and Optoelectronic Materials
Technical Institute of Physics and Chemistry
Chinese Academy of Sciences
Beijing 100190, China

 The ORCID identification number(s) for the author(s) of this article can be found under <https://doi.org/10.1002/smt.201900061>.

Dr. R. W. Shao, Dr. S. L. Chen, Prof. P. Gao
Electron Microscopy Laboratory, and International Center
for Quantum Materials
School of Physics
Peking University
Beijing 100871, China
E-mail: p-gao@pku.edu.cn

Prof. L. T. Sun, Prof. F. Xu
Center for Advanced Materials and Manufacture
Joint Research Institute of Southeast University and Monash University
Suzhou 215123, China

Prof. H. L. Xin
Department of Physics and Astronomy
University of California
Irvine, CA 94720, USA

DOI: 10.1002/smt.201900061

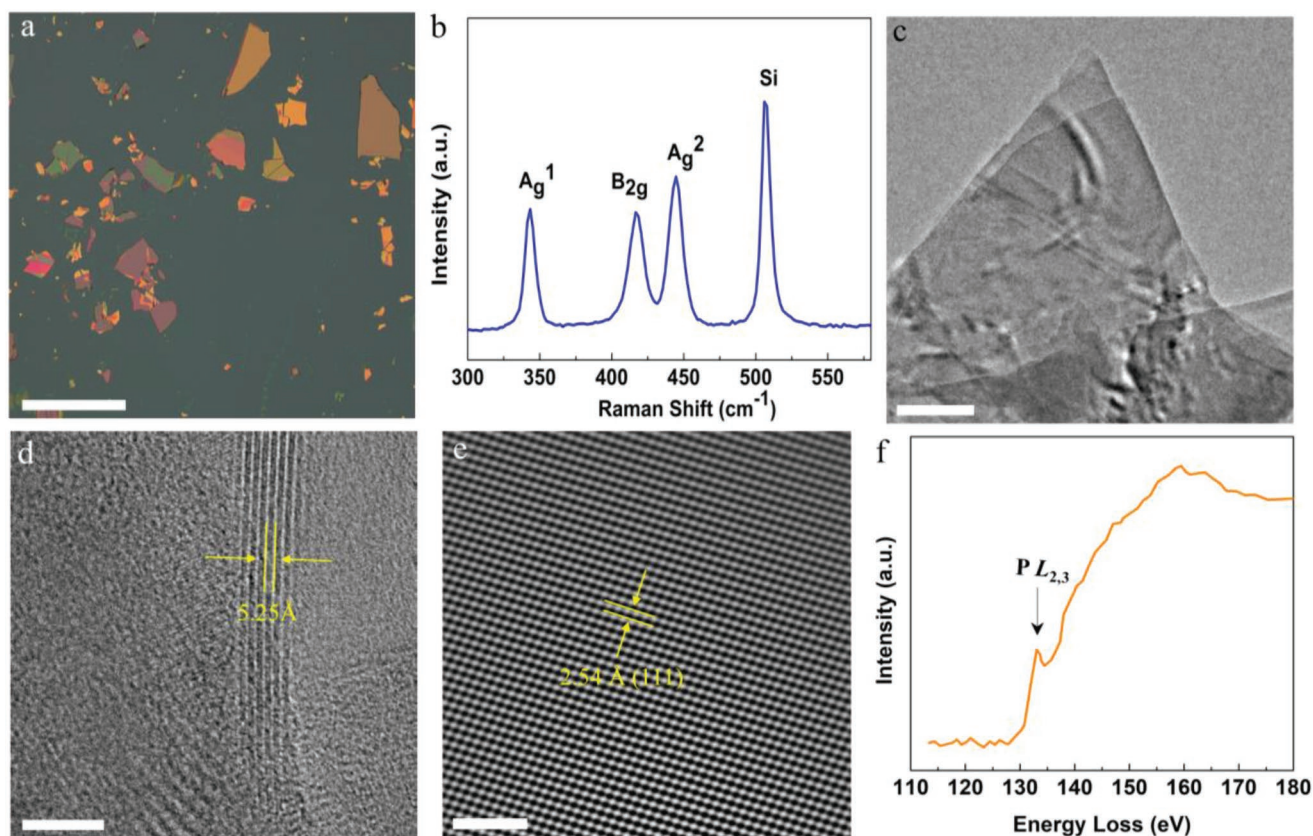


Figure 1. Structural characterizations of few-layer phosphorene nanosheet. a) Optical image of the mechanically exfoliated phosphorene samples, showing large numbers of phosphorene nanosheets with various size and thickness. b) Raman spectrum of the few-layer phosphorene nanosheet, characterized by the A_g^1 , B_{2g} , and A_g^2 modes of orthorhombic crystalline BP. c,d) Typical TEM images of the phosphorene sample. The lattice spacing of 0.52 nm corresponds to the interlayer distance ((002) plane) of BP, showing that the obtained phosphorene nanosheet is of few layers. e) HRTEM image of the few-layer phosphorene nanosheet. Both the ordered lattice and the FFT pattern confirm that the phosphorene sample is well-crystallized. f) EELS spectrum of the few-layer phosphorene nanosheet. The core-loss peak at 133 eV corresponds to the $P L_{2,3}$ edge. Scale bar: (a) 10 μm , (c) 200 nm, (d) 5 nm, and (e) 2 nm.

such underlying interfacial transport and electrochemistry, which would ultimately lead to mechanistic understanding of the intricate electrochemical reactions of batteries, is highly desirable but very challenging.

Recently, Huang group and Wang group have developed in situ transmission electron microscopy (TEM) technique for studying nanoscale electrochemical reactions.^[19,20] By using this technology, dynamic ion migration and concomitant phase transformation have been revealed for a great number of materials at an atomic scale and millisecond,^[21–24] providing us unprecedented opportunities to explore the interfacial ionic transport.

Herein, we investigate the solid–solid interfacial sodium ionic transport and electrochemical reaction between few-layer phosphorene nanosheets by virtue of state-of-the-art in situ TEM technique. Encouragingly, we have dynamically evidenced a reversible sodium ionic shuttling between phosphorene nanosheets in real time, accompanied with alternant volumetric expansion and contraction. Moreover, we reveal that the interfacial sodium transfer kinetics are closely related to the interface orientation and emphasize the significance of the intimate contact between solid electrodes in inhibiting dendrite growth. Furthermore, we probe the interfacial interactions

between adjacent phosphorene nanosheets by using high-resolution TEM and successfully track the multiple sodium ionic transport pathways in phosphorene with atomic resolution. We believe this work would provide valuable insights into understanding the solid–solid interfacial ionic transport and electrochemistry inside batteries.

2. Results and Discussion

Few-layer phosphorene was used for this study due to its rather high specific capacity ($\approx 2596 \text{ mAh g}^{-1}$) when alloying with sodium, enabling promising potential for rechargeable batteries.^[25,26] Moreover, phosphorene shares a similar layer structure to graphene, possessing both excellent electronic and ionic conductivities that facilitate the ionic diffusion in host structures.^[27–29] Prior to the in situ TEM experiment, few-layer phosphorene nanosheets were mechanically peeled off from black phosphorus (BP) crystal and then were transferred onto a half TEM Cu grid with carbon film. We verified the crystal structure of phosphorene nanosheets by using Raman spectrum (Figure 1a,b), where three prominent peaks at 362, 436, and 464 cm^{-1} can be indexed to the A_g^1 , B_{2g} , and A_g^2 modes of

the orthorhombic crystalline BP.^[30] Layered structure of phosphorene was subsequently confirmed by TEM measurement with folded edges (Figure 1c,d), which shows a lattice spacing of 0.52 nm, corresponding to the interlayer distance ((002) plane, JCPDS no. 74–1878) of BP. It also shows that the as-obtained phosphorene is of few layers and is well-crystallized, as corroborated by the high-resolution TEM (HRTEM) image (Figure 1d,e). The chemical quality of the few-layer phosphorene nanoflake is further checked by electron energy-loss spectroscopy (EELS) in Figure 1f, where the characteristic core-loss peak at 133 eV corresponding to the P $L_{2,3}$ edge is observed clearly.^[30] We note that the few-layer phosphorene nanosheet is relatively stable under the electron beam irradiation without obvious structural damage (Figure S1 and Movie S1, Supporting Information).

To investigate the interfacial ionic transport between solid phosphorene electrodes, we applied the in situ TEM experimental technique to deliberately design a nanoscale contact interface between few-layer phosphorene nanosheets. This strategy is slightly different from the conventional in situ TEM measurements on battery electrodes that were performed by making direct contact between Na₂O-coated sodium tip and the endpoint of an electrode material.^[31] Although the latter has advantages of precise control and dynamical characterization on sodiation of an individual nanostructure, it falls short on tracking interfacial ionic transport and electrochemical reactions between electrode materials, as illuminated in Figure 2a. Therefore, an appropriately modified open-cell in situ TEM technique that enables the interfacial investigation is badly necessary. Figure 2b illustrates the improved experimental configuration for investigating the interfacial ionic transfer and reactions between solid phosphorene nanosheets. It consists of a presodiated phosphorene (SP) nanosheet on tungsten (W) tip and a pristine phosphorene (PP) nanosheet on Cu grid. Briefly, the sodiation of few-layer phosphorene nanosheet was carried out by making direct contact with Na₂O/Na-coated W tip and applying a certain voltage (Figure S2, Supporting Information). We found after alloying with sodium the phosphorene nanosheet shows relatively poor mechanical property than the pristine one, so that it can be easily transferred by the W tip (Figure S3 and Movie S2, Supporting Information). Further moving such an SP nanosheet to touch another PP nanosheet, the nanoscale solid–solid contact interface was established. Figure 2c shows a typical TEM image of the nanoscale contact interface between phosphorene inside TEM.

Figure 2d–m presents the time-sequence TEM images of the interfacial sodium ionic transport between the SP and PP nanosheets, where the morphological and structural evolutions have been observed (Movie S3, Supporting Information). Before contact, the SP shows amorphous feature as indicated by the HRTEM image and the selected area electron diffraction (SAED) pattern with dispersive diffraction ring (Figure S4, Supporting Information). This is consistent with reported work that the structure of phosphorene finally changed into amorphous sodium phosphide (Na₃P) phase after a full sodiation.^[32,33] We note that the SP nanosheet is partially covered with extra sodium source particles, as indicated by the white arrow (Figure 2c), resembling a scenario inside a real battery. The PP nanosheet is slightly curved in the edge and its

x axis is identified by using high-resolution imaging (Figure S5, Supporting Information),^[25] while the y and z axes are uncertain due to lack of further evidence. When the SP nanosheet approaches the PP nanosheet, one sodium particle on the surface of the SP snaps slightly onto the PP as a result of the van der Waals attraction. After applying a small negative bias on the PP with respect to the SP, the sodium particle is gradually inserted into the PP, leading to the gray-contrast stripes across the surface of the PP nanosheet (Figure 2e).^[33] As the SP further moves forward, the sodium source and the SP nanosheet contact together with the PP nanosheet, resulting in the drastic sodiation reaction of the PP with 91% size elongation along the direction perpendicular to the x axis, whereas the dimension along the x axis remains nearly unchanged (Figure 2f). It has been suggested the full sodiation of few-layer phosphorene forming Na₃P phase has a theoretical volume expansion of 500% and the x and y axis expansions have been measured to be 0% and 92%, respectively.^[25] This means the full sodiation of the PP nanosheet. Energy dispersive X-ray spectroscopy (EDS) also reveals that the PP nanosheet has been fully sodiated with the 2.89:1 atomic ratio of Na and P, indicating the formation of Na₃P phase (Figure S6a, Supporting Information). Moreover, we can infer that the direction normal to the x axis is the y axis, and the z axis is along the thickness direction of the PP with a significant expansion of $\approx 160\%$. Such anisotropic expansions along the x , y , z axes are the result of the easier sodium ionic diffusion and the weaker P–P bonding along the x axis.^[25,33]

During the first sodiation of the PP nanosheet, it is worth noting that the SP nanosheet exhibits slight shrink in morphology, suggesting the migration of sodium ions from the SP to the PP via contact interface. This phenomenon is more prominent in the subsequent desodiation process of the PP when a reverse bias voltage is applied. As displayed in Figure 2g–i, the PP nanosheet shows apparent volume contraction upon desodiation, while the SP nanosheet expands simultaneously in volume, meaning the back-flow of sodium ions from the PP nanosheet to the SP nanosheet. The EDS spectrum also proves that the sodium ions are nearly extracted fully from the PP nanosheet since the atomic ratio of Na and P in the PP nanosheet is about 0.06:1 (Figure S6b, Supporting Information). Such reversible ionic shuttling is just like a scenario in inverting a sand clock back and forth, directly revealing the existence of interfacial ionic transport between solid phosphorene nanosheets. The SAED pattern shows that the desodiated PP nanosheet exhibits amorphous structure (Figure S7, Supporting Information). Although the PP nanosheet does not recover to its original crystalline state after desodiation, sodium ions can still insert into or extract from the PP nanosheet through the contact interface in subsequent electrochemical sodiation/desodiation cycles, inducing alternate volume expansion or contraction (Figure 2j–m). The EDS analysis shows that the atomic ratio of Na and P in the phosphorene nanosheet increases from the 0.06 to 2.58 after the second sodiation, and further decreases to 0.22 after the second desodiation (Figure S6c,d, Supporting Information). These results demonstrate that the reversible electrochemical cycles related with the alloying reactions are established between the amorphous phosphorene and amorphous Na₃P phases. We believe the fantastic interfacial sodium ionic transport is significantly facilitated by

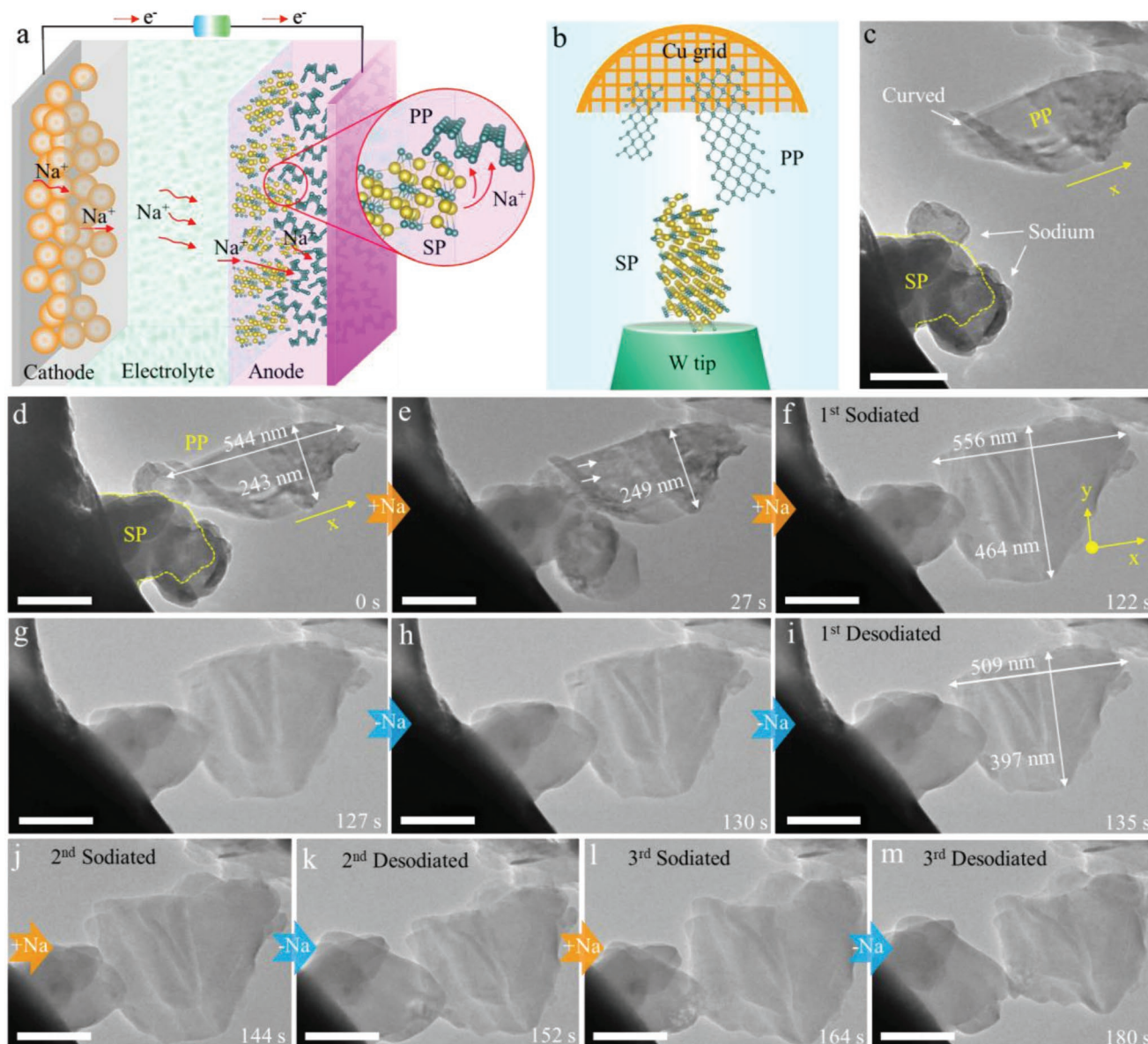


Figure 2. Reversible sodium transport between few-layer phosphorene nanosheets. a) The diffusion pathways of sodium ions in a battery during charging. The enlarged inset shows the underlying interfacial sodium ionic transport from the sodiated phosphorene nanosheet (SP) to the pristine phosphorene (PP) nanosheet. b) Schematic illustration of the in situ experimental setup, consisting of a SP nanosheet and a PP nanosheet. c) Typical TEM image of the as-established in situ contact interface between the SP and the PP nanosheets. d–f) Applying a bias drove the sodium ion diffusion from the SP to the PP. The former gradually shrank in volume, and the latter began to expand, like a balloon that air was being pumped into. g–i) After applying a reverse bias, the back-flow of sodium ion from the PP to the SP occurred. The former began to expand, and the latter gradually shrank in volume. j–m), Additional two cycles of sodium ionic transport through the contact interface, showing the reciprocating motion of sodium ions and the corresponding morphological evolution. Scale bar: (c–m) 200 nm.

the fast ionic conductivity of Na_3P . First-principles simulations have predicted that the Na_3P exhibits high ionic conductivity, in favor of the sodium diffusion with low energy barrier during desodiation.^[34] To the best of our knowledge, this is the first direct observation of interfacial mass transfer between solid electrodes, which may supply valuable insights into the intricate interfacial reactions inside batteries.

To gain in-depth knowledge of the solid–solid interfacial mass transfer, close inspection has been carried out on the contact interface. We find that sodium ions can transfer

unimpededly from one side to the other when contact interface is very solid, which has been verified by the distinct volume expansion and contraction in Figure 2. On the contrary, the interfacial migration of sodium ions would be impeded in the case of poor contact. As presented in Figure 3a,b and Movie S4 (Supporting Information), upon biasing, sodium transfer from the SP to the PP occurs accompanied by reverse change in their geometries. However, due to the instantaneous sodium migration, great strain is simultaneously imposed onto the interface, leading to the break

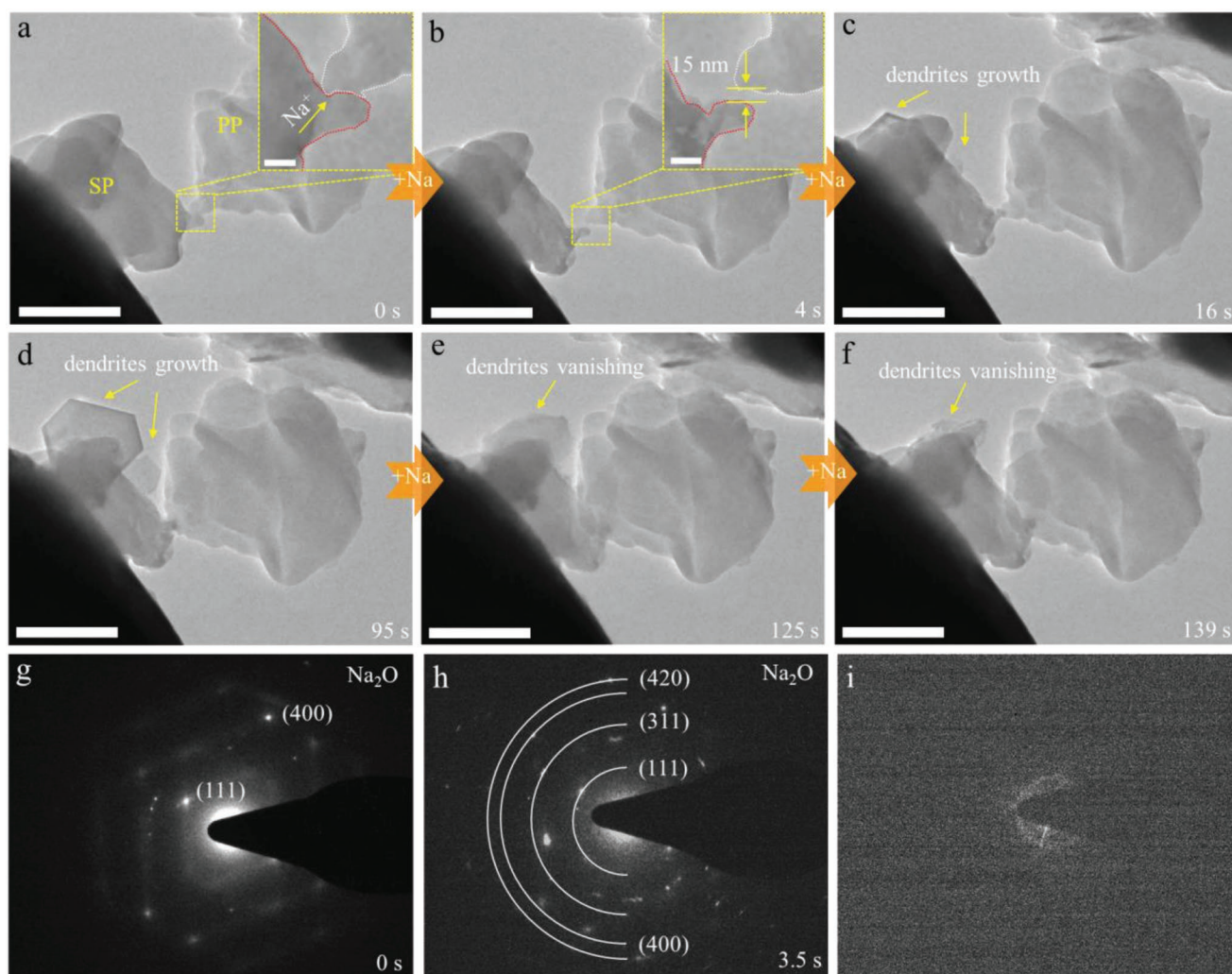


Figure 3. Contact interface-confined sodium transport between few-layer phosphorene nanosheets. a–f) TEM image series of the interfacial sodium transport upon biasing. (a) Line contact. (b) Break of contact with a gap of about 15 nm. (c,d) Growth of hexagonal dendrites. (e,f) Reconstruction of the contact interface and the vanishing of dendrites. g–i) Time-sequenced SAED patterns of the dendrites during the interfacial reactions, showing the formation and disappearance of Na_2O dendrites. Scale bar: (a–f) 200 nm; inset in (a) and (b) 20 nm.

of contact (inset in Figure 3b). It is worth noting that the extracted sodium ions, which have not been taken in by the PP nanosheet in time, gradually accumulate and recrystallize in the form of dendrites on the surface of SP nanosheet (denoted by yellow arrows in Figure 3c,d). Once the contact interface is rebuilt (Figure 3e,f), dendrites begin to vanish, revealing reliable ionic transport within solid electrodes. In Figure 3g–i, dendrites are identified to be Na_2O by using electron diffraction patterns, which are acquired from other contact situation. The formation of Na_2O is ascribed to the oxidation of sodium ions by the trace oxygen in the TEM chamber.^[35] In view of the difference between in situ experiment and real battery environment, analogous Na dendrites would grow in the latter, which not only exacerbates the consumption of Na metal but also brings about safety issues.^[36] Accordingly, our observations highlight that the intimate contact between components is necessary to facilitate smooth flow channels for ions within the whole electrodes.

It was recently reported that the sodium ion transport is preferred in zigzag edge rather than the armchair edge.^[33] This implies that contact orientation between adjacent nanosheets would exert an effect on the interfacial sodium transfer kinetics. In Figure 4 and Movies S5 and S6 (Supporting Information), we deliberately constructed two types of contact interfaces, which are normal to the zigzag direction (Figure 4a,b; Figure S8, Supporting Information) and parallel to the zigzag direction (Figure 4c–e; Figure S9, Supporting Information), respectively. As to the former, fast interfacial sodium ionic transport is favored upon contact, leading to the crystal-to-amorphous transformation of the PP nanosheet within 8 s. However, when the contact interface is parallel to the zigzag direction, no discernible sodiation is observed in the initial 50 s. Afterward, the sodiation stripes initiate along the zigzag direction (denoted by the red arrows) and meanwhile the large lateral expansion from 122 to 153 nm is observed (Figure 4d,e). Typically, the sodiation stripes are aroused by the insertion of sodium ions, indicating

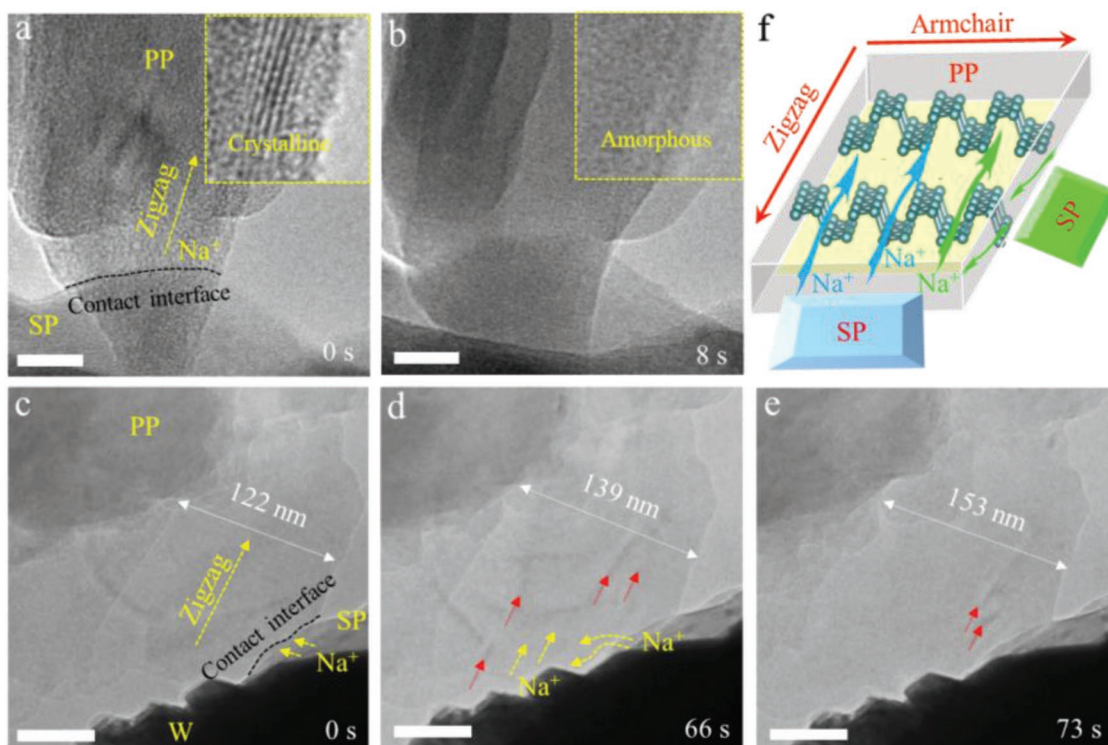


Figure 4. TEM image series of interfacial sodium transport with different contact orientations between the SP and the PP nanosheets. a,b) Contact interface normal to the zigzag direction. Fast sodium ionic transport is favored upon contact, leading to the crystal-to-amorphous transformation of the PP nanosheet within 8 s. c–e) Contact interface parallel to the zigzag direction. Sodium ions first migrate into diffusion channels along the zigzag direction, as indicated by the yellow arrows, and then embed into the PP structure, causing the sodiation stripes along the zigzag direction (marked by red arrows). f) Schematic diagram of the interfacial sodium transport with different contact geometries between the SP and the PP nanosheets. Scale bar: (a,b) 10 nm, (c–e) 50 nm.

that sodium ions first migrate into diffusion channels along the zigzag direction, as indicated by the yellow arrows, and then embed into the PP structure. This leads to overall sluggish kinetics for interfacial sodium migration. Based on these results, sodium ions prefer to diffuse along the zigzag direction regardless of the contact geometries, as schematically shown in Figure 4f.

Further probing the interfacial sodium ionic transport and the concomitant phase evolution would lead to mechanistic understanding of the underlying interfacial electrochemistry.^[22,37] Hence, we performed HRTEM to examine the atomic structures of interfaces and fully understand how the phosphorene electrode interact (Movie S7, Supporting Information). As shown in Figure 5a–d, upon insertion of sodium ions, the crystal structure of PP domain immediately changes into multiple phases. Thereinto the amorphous matrix suggests that the phosphorene has been fully sodiated into the Na_3P , of which the boundary can be distinguished by the white dashed line. With reaction going on, the boundary propagates forward progressively until the PP domain becomes amorphous totally. The relevant sodium migration rate is estimated to be $5.8 \text{ nm}^2 \text{ s}^{-1}$ (Figure S10, Supporting Information) by measuring the projected areas of the full reaction region versus the reaction time.

To determine the detailed electrochemical reactions at interfaces, localized phase transformations have been analyzed carefully. In Figure 5e–i, a series of Na_xP ($3 \geq x > 0$) intermediate

phases with atomic resolution have been successfully identified via HRTEM images and the FFT patterns. At the initial stage, the few-layer phosphorene (Figure 5e) with an orthorhombic structure ($Cmca$) changes to a locally stable NaP_5 - $Pnma$ phase (Figure 5f), which shows a 3D network with the majority of the P ions threefold bonded.^[38] This result suggests the cleavage of the P–P bond in the phosphorene, which is slightly distinct with the theoretical prediction that the layered structure of phosphorene can be maintained up to the composition of $\text{Na}_{0.25}\text{P}$.^[32] With the sodiation proceeding, (101) plane of the NaP_5 vanishes, and a new phase of Na_3P_{11} - $Pbcn$ is subsequently formed with isolated P_{11} cages dispersed in the 3D structure (Figure 5g).^[32] Further increasing the sodium content, the structures of the Na–P systems are significantly different, tending to form chains or broken chains (Figure 5h). Both the HRTEM image and the FFT pattern have verified the generation of the stable orthorhombic NaP - $P21/c$ phase at this stage. For higher sodium concentrations, the Na–P structures are formed by isolated P ions,^[32,38,39] which ultimately leads to the formation of an amorphous structure, that is, Na_3P matrix (Figure 5i). Although the alloying reactions of few-layer phosphorene with sodium have been widely studied though theoretical and experimental calculations,^[32,38–40] there is currently a lack of direct evidence. The present observations not only disclose the interfacial electrochemistry between solid–solid electrodes, but also clarify the whole reaction mechanism of few-layer phosphorene with sodium.

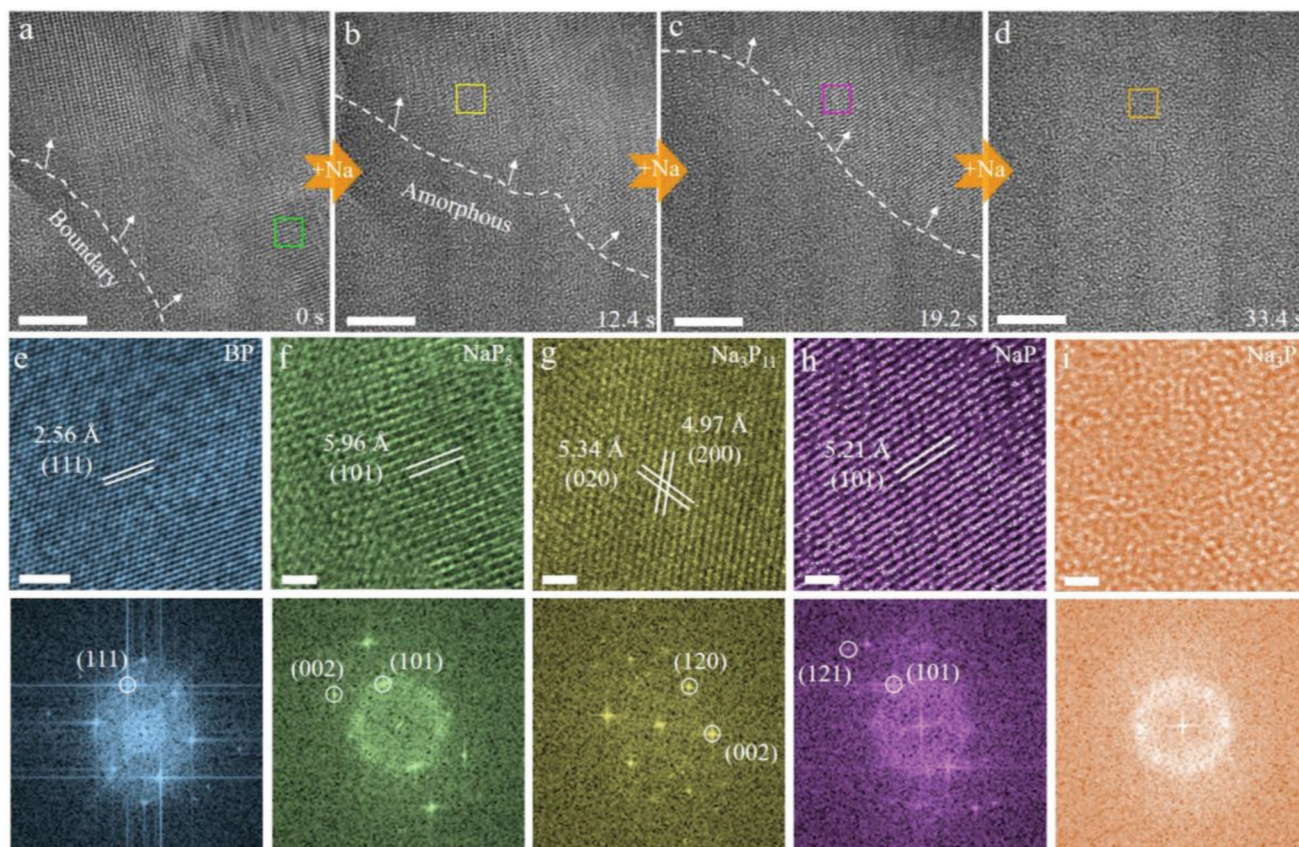


Figure 5. Atomically probing the structural evolution of few-layer phosphorene during interfacial sodium transport. a–d) Time-sequenced HRTEM images of the PP domain upon sodium insertion. The white dashed lines clearly denote the boundary of the domain of sodium insertion. e–i), Enlarged HRTEM images and the FFT patterns below corresponding to the squares in (a–d), demonstrating the formation of NaP_5 , Na_3P_{11} , NaP , and Na_3P intermediate phases respectively. Scale bar: (a–d) 10 nm, (e–i) 2 nm.

Figure 6 displays time-sequence HRTEM images of another PP domain during interfacial reactions, exhibiting unique stripe-like sodium transport pathways (Movie S8, Supporting Information). As shown in Figure 6a, upon biasing intermediate phase of NaP_5 has been identified by the HRTEM image and the FFT pattern, which is in accord with the result in Figure 5. Later, the NaP_5 changes into Na_3P_{11} as a result of the further alloying reaction with the embedded sodium ions, confirmed by the appearance of the diffraction spots from orthorhombic Na_3P_{11} (indicated by yellow circles, inset in Figure 6b). We note the formation of Na_3P_{11} gives rise to the shallower contrast in the NaP_5 lattices, as denoted by the yellow arrows in Figure 6b, which further evolves into amorphous Na_3P with stripe-like patterns (Figure 6c). Such unique stripe-like sodium transport pathways mean that the sodium ions selectively transport along the [101] direction of NaP_5 , which is likely attributed to the sluggish interfacial sodium transport kinetics, or the structural defects inside the host of NaP_5 that facilitate the migration of the sodium ions.^[41] With further sodium insertion, more stripes emerge at the expense of NaP_5 lattices. Simultaneously, the diffraction spots of both the NaP_5 and Na_3P_{11} become weaker and ultimately disappear at 18.4 s (Figure 6d–f), suggesting the full amorphization of the PP domain. The total area of striped domains in this selected region is plotted as a function of time in Figure 2h, confirming that the sodiation proceeds slowly at the initial and then quickly with

more sodiation stripes. Figure 6g shows the split process of the diffraction spot (102) of NaP_5 phase during interfacial reactions. The split of (102) reflection between pristine and reacted phase is measured to be $\approx 4.2\%$, which originates from the sodium insertion-induced lattice expansion.

3. Conclusion

In conclusion, we have revealed reversible interfacial sodium ionic transport between few-layer phosphorene electrodes in real space by state-of-the-art in situ TEM technique. Our observations have demonstrated that the sodium ions were able to shuttle reversibly between adjacent phosphorene nanosheets and found such unique interfacial ionic transport behaviors are significantly related to the area and orientation of the contact interface. Further, we have successfully visualized multiple sodium transport pathways in phosphorene at the atomic scale and identified distinct intermediate phases at various reaction stages. Additionally, the unique stripe-like sodiation pathways were also revealed due to the insufficient sodium sources and the structural defects. We believe the present study discloses a brand new interfacial electrochemistry inside batteries and provides in-depth knowledge on reaction mechanism of phosphorene electrodes.

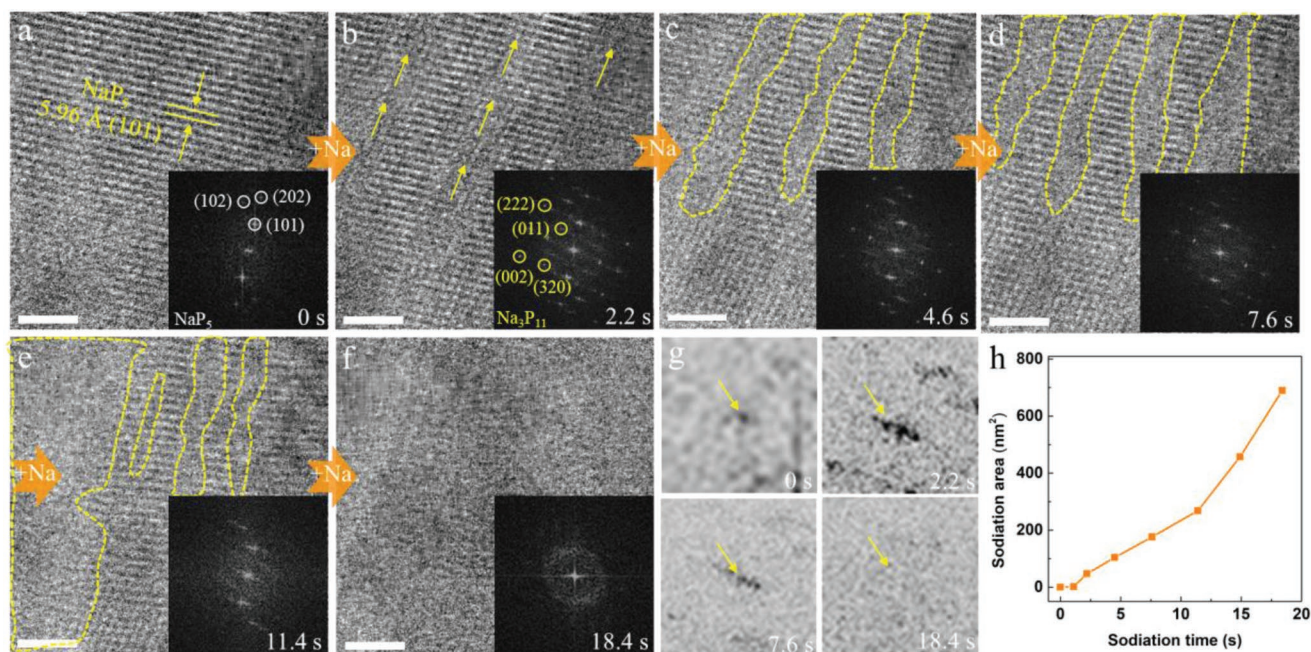


Figure 6. Tracking the stripe-like sodium transport pathway in few-layer phosphorene domain. a) HRTEM image of the phosphorene domain after sodium insertion and the corresponding FFT pattern below, suggesting the formation of NaP₅. b–f) The structural evolution and the corresponding FFT patterns during further sodium insertion, exhibiting a unique stripe-like sodium transport pattern, as indicated by the yellow dashed lines. g) The split process of the diffraction spot (102) of NaP₅, suggesting the lattice expansion induced by the sodium insertion. h) The total striped domain area is plotted as a function of time from the selected region. Scale bar: (a–e) 5 nm.

4. Experimental Section

In Situ Configuration: To obtain few-layer phosphorene nanosheets, multilayer phosphorene nanosheets were first mechanically exfoliated onto polydimethylsiloxane (PDMS) stamp from black phosphorus crystal (Smart Elements, product no. 003058). Then the PDMS stamp with multilayer phosphorene nanosheets was brought to contact with Si/SiO₂ substrate and was heated together at 90 °C for 1 min by applying gentle pressure on PDMS stamp. After that, the PDMS stamp was removed, ensuring residue-free surface of few-layer phosphorene nanosheets on the Si/SiO₂ substrate. Few-layer phosphorene nanosheets electrode was obtained by using a half TEM Cu grid covered with carbon films to scratch the surface of few-layer phosphorene nanosheets on the Si/SiO₂ substrate. Metallic sodium was attached to the tungsten tip by scratching the tip across the surface of bulk sodium. After that, the few-layer phosphorene nanosheets-dispersed Cu grid and the sodium-coated tungsten tip were loaded into a specimen holder, acting as the working electrode and counter electrode, respectively. All operations were conducted in the argon-filled glove box to prevent excessive oxidation of the sodium metal. During the holder transfer into the TEM chamber, a thin Na₂O layer naturally grew on the surface of sodium metal, which functioned as a solid electrolyte. The piecontrolled movement was operated at single nanosheet level inside TEM to make the Na/Na₂O contact the few-layer phosphorene nanosheet. Afterward, a constant negative bias was applied on the few-layer phosphorene nanosheet with respect to the Na/Na₂O, so as to initiate the electrochemical sodiation of phosphorene. For further investigation of interfacial sodium ionic transport between few-layer phosphorene nanosheets, the sodiated phosphorene nanosheet was deliberately transferred by tungsten tip and such a fully sodiated phosphorene nanosheet was moved to touch another pristine few-layer phosphorene nanosheet, forming the desired contact interface. The subsequent interfacial electrochemical reactions were actuated by applying appropriate bias. During the observation, the electron beam was spread out to avoid beam effects.

In situ TEM experiments (Figures 2,3, and 4) were performed at aberration-corrected Titan microscope (FEI Titan 80–300), which is operated at an acceleration voltage of 300 kV and installed with a CCD camera with frame rates up to 5 frames per second. Nanofactory piezocontrolled TEM-STEM sample holder was used to construct the nanosized sodium-ion battery. In situ HRTEM experiments (Figures 5 and 6) were carried out using Tecnai F20 at 200 kV equipped with an OneView IS (Gatan) camera with frame rates of 25 frames per second. An electrical TEM specimen holder (PicoFemto) was used to build the nanosized sodium-ion battery inside TEM.

Supporting Information

Supporting Information is available from the Wiley Online Library or from the author.

Acknowledgements

C.Y.Z. and R.W.S. contributed equally to this work. This work was supported by the National Natural Science Foundation of China (Grant Nos. 11774051, 51502007, and 61574034), the 973 Program (Grant No. 2015CB352106), the National Key R&D Program of China (Grant Nos. 2016YFA0300804 and 2016YFA0300903), National Equipment Program of China (ZDYZ2015-1), the Fundamental Research Funds for the Central Universities (2242018K41020 and 2242018k1G012), and Scientific Research Foundation of Graduate School of Southeast University (YBPY1709). The authors acknowledge the Electron Microscopy Laboratory in Peking University for the use of in situ TEM platform.

Conflict of Interest

The authors declare no conflict of interest.

Keywords

electrochemistry, in situ TEM, interfacial ionic transport, phosphorene, rechargeable batteries

Received: January 22, 2019

Revised: April 14, 2019

Published online: May 15, 2019

- [1] A. V. Akimov, R. Asahi, R. Jinnouchi, O. V. Prezhdo, *J. Am. Chem. Soc.* **2015**, *137*, 11517.
- [2] Y. Y. Hu, Z. G. Liu, K. W. Nam, O. J. Borkiewicz, J. Cheng, X. Hua, M. T. Dunstan, X. Q. Yu, K. M. Wiaderek, L. S. Du, K. W. Chapman, P. J. Chupas, X. Q. Yang, C. P. Grey, *Nat. Mater.* **2013**, *12*, 1130.
- [3] J. C. Bachman, S. Muy, A. Grimaud, H. H. Chang, N. Pour, S. F. Lux, O. Paschos, F. Maglia, S. Lupart, P. Lamp, L. Giordano, Y. Shao-Horn, *Chem. Rev.* **2016**, *116*, 140.
- [4] H. P. Zhou, Q. Chen, G. Li, S. Luo, T. Song, H. Duan, Z. R. Hong, J. B. You, Y. S. Liu, Y. Yang, *Science* **2014**, *345*, 542.
- [5] H. Schmidt, F. Giustino, G. Eda, *Chem. Soc. Rev.* **2015**, *44*, 7715.
- [6] A. Marchetti, J. Chen, Z. F. Pang, S. H. Li, D. S. Ling, F. Deng, X. Q. Kong, *Adv. Mater.* **2017**, *29*, 1605895.
- [7] J. Ma, P. Hu, G. L. Cui, L. Q. Chen, *Chem. Mater.* **2016**, *28*, 3578.
- [8] X. G. Han, Y. H. Gong, K. Fu, X. F. He, G. T. Hitz, J. Q. Dai, A. Pearce, B. Y. Liu, H. Wang, G. Rublo, Y. F. Mo, V. Thangadurai, E. D. Wachsman, L. B. Hu, *Nat. Mater.* **2017**, *16*, 572.
- [9] D. K. Takamatsu, Y. Koyama, Y. Orikasa, S. Mori, T. Nakatsutsumi, T. Hirano, H. Tanida, H. Arai, Y. Uchimoto, Z. Ogumi, *Angew. Chem., Int. Ed.* **2012**, *51*, 11597.
- [10] B. B. Wu, S. Y. Wang, W. J. EvansIV, D. Z. Deng, J. H. Yang, J. Xiao, *J. Mater. Chem. A* **2016**, *4*, 15266.
- [11] C. Ma, Y. Q. Cheng, K. B. Yin, J. Luo, A. Sharafi, J. Sakamoto, J. C. Li, K. L. More, N. J. Dudney, M. F. Chi, *Nano Lett.* **2016**, *16*, 7030.
- [12] C. Ma, K. Chen, C. D. Liang, C. Nan, R. Ishikawa, K. More, M. F. Chi, *Energy Environ. Sci.* **2014**, *7*, 1638.
- [13] N. Ohta, K. Takada, L. Zhang, R. Ma, M. Osada, T. Sasaki, *Adv. Mater.* **2006**, *18*, 2226.
- [14] K. Takada, *Langmuir* **2013**, *29*, 7538.
- [15] K. Takada, N. Ohta, L. Q. Zhang, X. X. Xu, B. T. Hang, T. Ohnishi, M. Osada, T. Sasaki, *Solid State Ionics* **2012**, *225*, 594.
- [16] T. Okumura, T. Nakatsutsumi, T. Ina, Y. Orikasa, H. Arai, T. Fukutsuka, Y. Iriyama, T. Uruga, H. Tanida, Y. Uchimoto, Z. Ogumi, *J. Mater. Chem.* **2011**, *21*, 10051.
- [17] A. Sakuda, A. Hayashi, M. Tatsumisago, *Chem. Mater.* **2010**, *22*, 949.
- [18] Q. B. Zhang, K. B. Yin, H. Dong, Y. L. Zhou, X. D. Tan, K. H. Yu, X. H. Hu, T. Xu, C. Zhu, W. W. Xia, F. Xu, H. M. Zheng, L. T. Sun, *Nat. Commun.* **2017**, *8*, 14889.
- [19] J. Y. Huang, L. Zhong, C. M. Wang, J. P. Sullivan, W. Xu, L. Q. Zhang, S. X. Mao, N. S. Hudak, X. H. Liu, A. Subramanian, H. Y. Fan, L. Qi, A. Kushima, J. Li, *Science* **2010**, *330*, 1515.
- [20] Y. J. Zhu, J. W. Wang, Y. Liu, X. H. Liu, A. Kushima, Y. H. Liu, Y. H. Xu, S. X. Mao, J. Li, C. S. Wang, J. Y. Huang, *Adv. Mater.* **2013**, *25*, 5461.
- [21] F. Xu, L. J. Wu, Q. P. Meng, M. Kaltak, J. P. Huang, J. L. Durham, M. Fernandez-Serra, L. T. Sun, A. C. Marschilok, E. S. Takeuchi, K. J. Takeuchi, M. S. Hybertsen, Y. M. Zhu, *Nat. Commun.* **2017**, *8*, 15400.
- [22] J. Zhou, J. C. Chen, M. X. Chen, J. Wang, X. Z. Liu, B. Wei, Z. C. Wang, J. J. Li, L. Gu, Q. H. Zhang, H. Wang, L. Guo, *Adv. Mater.* **2019**, *31*, 1807874.
- [23] Y. X. Huang, C. Y. Zhu, S. L. Zhang, X. M. Hu, K. Zhang, W. H. Zhou, S. Y. Guo, F. Xu, H. B. Zeng, *Nano Lett.* **2019**, *19*, 1118.
- [24] L. Q. Zhang, Y. S. Tang, Y. C. Wang, Y. L. Duan, D. G. Xie, C. Y. Wu, L. S. Cui, Y. F. Li, X. H. Ning, Z. W. Shan, *RSC Adv.* **2016**, *6*, 96035.
- [25] J. Sun, H. Lee, M. Pasta, H. T. Yuan, G. Y. Zheng, Y. M. Sun, Y. Z. Li, Y. Cui, *Nat. Nanotechnol.* **2015**, *10*, 980.
- [26] Y. Q. Fu, Q. L. Wei, G. X. Zhang, S. H. Sun, *Adv. Energy Mater.* **2018**, *8*, 1702849.
- [27] Y. Zhang, Y. Zheng, K. Rui, H. H. Hng, K. Hippalgaonkar, J. W. Xu, W. P. Sun, J. X. Zhu, Q. Y. Yan, W. Huang, *Small* **2017**, *13*, 1700661.
- [28] V. V. Kulish, O. I. Malyi, C. Persson, P. Wu, *Phys. Chem. Chem. Phys.* **2015**, *17*, 13921.
- [29] W. F. Li, Y. M. Yang, G. Zhang, Y. W. Zhang, *Nano Lett.* **2015**, *15*, 1691.
- [30] P. Yasaei, B. Kumar, T. Foroozan, C. H. Wang, M. Asadi, D. Tuschel, J. Ernesto Indacochea, R. F. Klie, A. Salehi-Khojin, *Adv. Mater.* **2015**, *27*, 1887.
- [31] C. Y. Zhu, F. Xu, H. H. Min, Y. Huang, W. W. Xia, Y. T. Wang, Q. Y. Xu, P. Gao, L. T. Sun, *Adv. Funct. Mater.* **2017**, *27*, 1606163.
- [32] K. P. S. S. Hembram, H. Jung, B. C. Yeo, S. J. Pai, S. Kim, K. Lee, S. S. Han, *J. Phys. Chem. C* **2015**, *119*, 15041.
- [33] A. Nie, Y. C. Cheng, S. C. Ning, T. Foroozan, P. Yasaei, W. Li, B. Song, Y. F. Yuan, L. Chen, A. Salehi-Khojin, F. Mashayek, R. Shahbazian-Yassar, *Nano Lett.* **2016**, *16*, 2240.
- [34] X. F. Yu, G. Giorgi, H. Ushiyama, K. Yamashita, *Chem. Phys. Lett.* **2014**, *612*, 129.
- [35] S. Meng, J. B. Wu, L. G. Zhao, H. Zheng, S. F. Jia, S. S. Hu, W. W. Meng, S. Z. Pu, D. S. Zhao, J. B. Wang, *Chem. Mater.* **2018**, *30*, 7306.
- [36] Y. Z. Li, Y. B. Li, A. Pei, K. Yan, Y. M. Sun, C. L. Wu, L. Joubert, R. Chin, A. L. Koh, Y. Yu, J. Perrino, B. Butz, S. Chu, Y. Cui, *Science* **2017**, *358*, 506.
- [37] R. W. Shao, S. L. Chen, Z. P. Dou, J. M. Zhang, X. M. Ma, R. Zhu, J. Xu, P. Gao, D. P. Yu, *Nano Lett.* **2018**, *18*, 6094.
- [38] M. Dahbi, N. Yabuuchi, M. Fukunishi, K. Kubota, K. Chihara, K. Tokiwa, X. Yu, H. Ushiyama, K. Yamashita, J. Son, Y. Cui, H. Oji, S. Komaba, *Chem. Mater.* **2016**, *28*, 1625.
- [39] M. Mayo, K. J. Griffith, C. J. Pickard, A. J. Morris, *Chem. Mater.* **2016**, *28*, 2011.
- [40] L. E. Marbella, M. L. Evans, M. F. Groh, J. Nelson, K. J. Griffith, A. J. Morris, C. P. Grey, *J. Am. Chem. Soc.* **2018**, *140*, 7994.
- [41] Y. H. Li, J. X. Lu, X. P. Cheng, H. F. Shi, Y. F. Zhang, *Nano Energy* **2018**, *48*, 441.